



**HAL**  
open science

# Chemical Looping Selective Oxidation of H<sub>2</sub>S using V<sub>2</sub>O<sub>5</sub> Impregnated over Different Supports as Oxygen Carriers

Tanushree Kane, Jesús Guerrero Caballero, Axel Löfberg

► **To cite this version:**

Tanushree Kane, Jesús Guerrero Caballero, Axel Löfberg. Chemical Looping Selective Oxidation of H<sub>2</sub>S using V<sub>2</sub>O<sub>5</sub> Impregnated over Different Supports as Oxygen Carriers. ChemCatChem, 2020, ChemCatChem, 12 (9), pp.2569-2579. 10.1002/cctc.201902031 . hal-02965559

**HAL Id: hal-02965559**

**<https://hal.univ-lille.fr/hal-02965559v1>**

Submitted on 13 Oct 2020

**HAL** is a multi-disciplinary open access archive for the deposit and dissemination of scientific research documents, whether they are published or not. The documents may come from teaching and research institutions in France or abroad, or from public or private research centers.

L'archive ouverte pluridisciplinaire **HAL**, est destinée au dépôt et à la diffusion de documents scientifiques de niveau recherche, publiés ou non, émanant des établissements d'enseignement et de recherche français ou étrangers, des laboratoires publics ou privés.

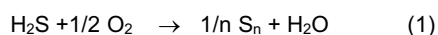
# Chemical looping selective oxidation of H<sub>2</sub>S using V<sub>2</sub>O<sub>5</sub> impregnated over different supports as oxygen carriers

Tanushree Kane<sup>[a]</sup>, Jesús Guerrero Caballero<sup>[a]</sup> and Axel Löfberg<sup>\*[a]</sup>

**Abstract:** Chemical looping concept is proposed to improve the efficiency of selective oxidation of H<sub>2</sub>S into elemental sulfur. V<sub>2</sub>O<sub>5</sub> as an active oxygen carrier, is impregnated on different supports and exposed cyclically to reductant (H<sub>2</sub>S) and to oxidant (O<sub>2</sub>). Among all, TiO<sub>2</sub> and SiO<sub>2</sub> proved as better supports for V<sub>2</sub>O<sub>5</sub> as they provided more formation of elemental sulfur than undesired SO<sub>2</sub> in the reductant step. Results indicate that the support can either directly react and provide oxygen to the process like for CeO<sub>2</sub> or indirectly affect the properties of the active phase, leading either into the improvement, as for TiO<sub>2</sub> and SiO<sub>2</sub>, or worsening, as in case of Al<sub>2</sub>O<sub>3</sub> and ZrO<sub>2</sub>. Oxygen carriers with partially reduced species, i.e., the combination of V<sup>5+</sup> and V<sup>4+</sup>, show better performances than carriers containing mostly highly oxidized V<sup>5+</sup> species. Interaction between the active phase and support plays a vital role for the controls of the formation of these partially reduced species.

## Introduction

Current strict environmental regulations force to treat the H<sub>2</sub>S emissions from the petroleum refineries and gas plants. Claus and super Claus processes are well-known desulfurization processes; however, due to the thermodynamic limitations, only 98% of H<sub>2</sub>S is converted into S. Hence, selective oxidation of hydrogen sulfide, avoiding the formation of SO<sub>2</sub>, is attractive according to the reaction:



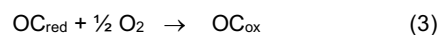
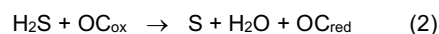
Selective oxidation to S is an exothermic reaction with no equilibrium limitations, unlike the Claus process. However, side reactions such as sulfur deposition on the catalyst and complete oxidation of H<sub>2</sub>S to SO<sub>2</sub> are responsible for the loss of sulfur yield in co-feed oxidation processes. These strongly depend upon the nature of the catalysts.

Different vanadium-based catalysts have already been studied in the past. Mainly, the bulk V<sub>2</sub>O<sub>5</sub> phase has been reported to have a better performance than other bulk oxides like magnesium oxide, bismuth oxide, and molybdenum oxide, iron oxide.<sup>[1-5]</sup> Supported,<sup>[1,6-8]</sup> and unsupported<sup>[9]</sup> vanadium oxides have been considered as catalysts for the selective oxidation of H<sub>2</sub>S. Vanadium oxides supported on silica,<sup>[10,11]</sup> alumina,<sup>[8,12,13]</sup>

titania,<sup>[5,11]</sup> zeolite,<sup>[14]</sup> and Ti pillared mormorillonite have been recently reported.<sup>[15]</sup> Vanadium based catalysts are thus active and selective for the oxidation of H<sub>2</sub>S to sulfur at relatively low temperatures. Acidic properties of the support and their effect on the interactions with the active phase were studied.<sup>[7,16,17]</sup> Supported vanadium oxide catalysts are significant in industrial processes. In many cases, they are doped with promoters to improve their activity and/or selectivity, and supports are used to improve mechanical strength, thermal stability, and lifetime.<sup>[18]</sup> Various studies<sup>[5, 8, 19, 20]</sup> showed that the dispersion of vanadium on different supports plays a vital role in the selective oxidation reaction of H<sub>2</sub>S. It has been reported that the TiO<sub>2</sub>-supported vanadium catalyst displayed much better redox characteristics compared to those supported on SiO<sub>2</sub>, resulting in better stable catalytic activity.

The chemical looping approach is well known for different oxidation reactions. This process involves an oxygen carrier, which is reduced in the presence of the reductant and produces the desired product. The reduced solid is subsequently exposed to an oxidant, which allows the carrier to be re-oxidized and regenerated. It should be underlined that the oxygen carrier material is an actual reactant and not catalysts.<sup>[21, 22]</sup> With respect to classical co-feed fixed systems, original reactor designs are necessary. Circulating fluidized bed systems or fixed bed switching reactors have mostly been used in the case of solid oxygen carriers and gas-phase reactants chemical looping.<sup>[23]</sup> For experimental studies in the laboratory scale, a fixed bed reactor fed alternatively with the gas reactants is usually the most appropriate.

Chemical looping processes have been studied for various application reactions of industrial interest, such as reforming<sup>[24,25]</sup> or combustion.<sup>[26, 27]</sup> We have recently extended the concept to selective oxidation of H<sub>2</sub>S to elemental.<sup>[22]</sup> It consists of separating equation (1) in two steps:



where "OC" represents the oxygen carrier.

With respect to direct, co-feed, oxidation reaction (1), chemical looping approach offers significant advantages:

- selectivity can be improved by avoiding direct reactions between H<sub>2</sub>S and oxygen from the gas phase offering better selectivity by favoring the reactivity of lattice oxygen species;
- sulfur deposited on the surface of the carrier can be removed during regeneration step thus limiting the deactivation;
- safety of the process is improved due to the absence of H<sub>2</sub>S: O<sub>2</sub> mixing.

We have shown that V<sub>2</sub>O<sub>5</sub> can act as an efficient oxygen carrier due to its oxygen mobility and storage capacity. However, due to

[a] Dr T. Kane, Dr J. Guerrero, Dr A. Löfberg  
UMR 8181 – UCCS – Unité de Catalyse et Chimie du Solide  
Univ. Lille, CNRS, Centrale Lille, Univ. Artois  
F-59000 Lille (France)  
E-mail: axel.lofberg@univ-lille.fr

the low temperature at which the reaction is carried out (typically between 150 and 200 °C), it was shown that a limited amount of oxygen species from the carrier were involved in the redox process due to the large size of particles. For instance, a few monolayers were concerned and not bulk species.<sup>[20]</sup>

The use of supported V<sub>2</sub>O<sub>5</sub> is therefore expected to provide better usage of oxygen species from the carrier. In this work, we propose a survey of several potential support materials (TiO<sub>2</sub>, SiO<sub>2</sub>, Al<sub>2</sub>O<sub>3</sub>, ZrO<sub>2</sub>, CeO<sub>2</sub>). This is performed by studying the reactivity of several supported V<sub>2</sub>O<sub>5</sub> to that of bulk oxide in given reaction conditions (T = 150 and 200 °C, 2000 ppm of H<sub>2</sub>S, H<sub>2</sub>S: O<sub>2</sub> ratio at 1:5).

A detailed description of experimental procedures for carrier synthesis, sample characterizations, and chemical looping reaction is provided in the Experimental Section.

## Results and Discussion

The active phase (V<sub>2</sub>O<sub>5</sub>) was impregnated on synthesized or commercial supports. Impregnated solids were then characterized by X-ray diffraction (XRD), X-ray photoelectron spectroscopy (XPS), N<sub>2</sub> adsorption/desorption measurements (BET), Temperature programmed reduction (TPR), and by Raman analysis.

### Characterization of bulk and supported oxygen carriers

#### Textural and structural characterization

Table 1 summarizes the properties of the different supports. SiO<sub>2</sub> and TiO<sub>2</sub> present the lowest surface areas and, coherently, the largest pore size. The silica surface area is rather low for such support, but the preparation method was not optimized to obtain high specific surface area materials. Commercial alumina shows the highest surface area.

As expected for such high active phase loading, i.e., 25 wt%, surface area and pore volume of the solids decrease after impregnation of V<sub>2</sub>O<sub>5</sub> on all supports. Whereas in the case of pore size, it increases after loading, but the trend is almost similar as in the respective supports. Figure 1 shows the XRD diffractograms of samples and reveals the presence of V<sub>2</sub>O<sub>5</sub> species on all support irrespective of their surface area and nature. This is because of the high loading of the V<sub>2</sub>O<sub>5</sub> present in the systems. It is observed that the Al<sub>2</sub>O<sub>3</sub>, CeO<sub>2</sub>, and ZrO<sub>2</sub> based solids present almost the same average crystallite size of V<sub>2</sub>O<sub>5</sub> (around 50-60 nm) irrespective of the crystallite size or surface area of the support (Table 2). For SiO<sub>2</sub> based carrier, the crystallite size of the V<sub>2</sub>O<sub>5</sub> is 87 nm.

Before reaction, V<sub>2</sub>O<sub>5</sub> over TiO<sub>2</sub> exhibits a sharp peak at 2 $\theta$  = 25.28°, which represents the (1 0 1) plane of the tetrahedral structure of TiO<sub>2</sub>, with reference to the JCPDF file (PDF 00-021-1272). Vanadium present on the support is in the orthorhombic structure of V<sub>2</sub>O<sub>5</sub> (PDF 00-041-1426) with the peak present at 20.7° corresponding to the plane (0 0 1). A low intense peak at 21.5° corresponding to the (2 0 0) plane and at 27.7° attributed to the V<sub>4</sub>O<sub>9</sub> with (PDF 23-0720) also shown by M.D. Soriano et al.,<sup>[28]</sup>

J.A. Cecilia et al.<sup>[29]</sup> and by J.P. Holgado et al.<sup>[30]</sup> and R. Nilsson et al.<sup>[31]</sup> or also coincide with the 2 $\theta$ =27.7° can be observed and could be attributed to VO<sub>2</sub> (0 1 0) plane according to JCPDF file PDF 04-003-2035.<sup>[22]</sup>

After reaction, V<sub>2</sub>O<sub>5</sub> over TiO<sub>2</sub> exhibits similar peaks as before reaction; however, the peak at 28.1° appears which is attributed to the (1 0 3) plane of V<sub>4</sub>O<sub>9</sub>.

Before reaction, V<sub>2</sub>O<sub>5</sub> over SiO<sub>2</sub> exhibits the intense peaks of only V<sub>2</sub>O<sub>5</sub> due to the amorphous nature of support SiO<sub>2</sub>.

After the reaction, SiO<sub>2</sub> supported carrier shows a significant lowering of the intensity of peak of V<sub>2</sub>O<sub>5</sub> and the appearance of the intense peaks at 27.7° attributed to the (2 0 2) plane and 56.02° attributed to the V<sub>4</sub>O<sub>9</sub> with PDF 23-0720. Other less intense peaks at 2 $\theta$  = 13.7, 21.3, 21.7, 28.1 also suggest the presence of V<sub>4</sub>O<sub>9</sub>, as shown by J.P. Holgado et al.<sup>[30]</sup> and R. Nilsson et al.<sup>[31]</sup>

For the V<sub>2</sub>O<sub>5</sub>-Al<sub>2</sub>O<sub>3</sub> sample before reaction, peaks at 37.6° and 67.5° illustrate the presence of the cubic form of the Al<sub>2</sub>O<sub>3</sub> with coincides with the PDF 46-1215. Apart from that, the XRD pattern shows the peaks for orthorhombic V<sub>2</sub>O<sub>5</sub> with an intense peak at 2 $\theta$  = 20.26. The intense peak represents the typical plane of (1 0 1) PDF 00-041-1426. However, the intense peak of the V<sub>2</sub>O<sub>5</sub> disappears after the reaction, whereas intense peaks of V<sub>4</sub>O<sub>9</sub> are present PDF 23-0720.

In the case of ZrO<sub>2</sub> supported carrier, the peaks present at 34.5° and 35.2° are representative of the (0 0 2) and (1 1 0) planes of ZrO<sub>2</sub> with reference to PDF 79-1769. Presence of V<sub>2</sub>O<sub>5</sub> characteristic peaks with reference to the PDF 00-041-1426 are observed before and after the reaction, while reduced form of vanadium oxide cannot be observed even after the chemical looping reaction.

Ceria-based solid XRD shows sharp peaks at 18.12° and 24.03° corresponding to (1 0 1) to (2 0 0) planes, respectively, of the tetragonal structure of CeVO<sub>4</sub> PDF 00-012-0757. This is an evidence for the formation of the mixed oxide of Ce and V. Along with it, strong intense peaks of the CeO<sub>2</sub> are also present at 28.55° and 33.08° representing the (1 1 1) and (2 0 0) planes of cubic structure, respectively. V<sub>2</sub>O<sub>5</sub> is also present on the support in the form of the orthorhombic structure with diffraction peaks at 20.3° and 26.3°.

After the reaction, zirconia based solid shows the presence of the identical peaks, indicating that no considerable evolution of the solid occurs during the reaction.

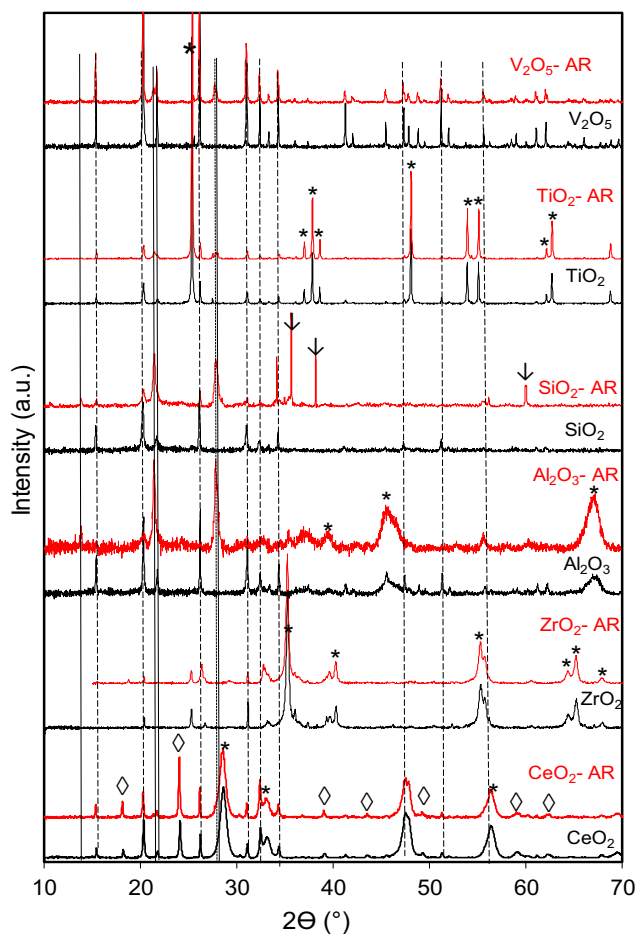


**Figure 1.** XRD study for bulk or supported (25 wt%  $V_2O_5$ ) oxygen carriers before and after the reaction, ( . . . )  $VO_2$ , ( — )  $V_4O_9$ , ( - - - )  $V_2O_5$ , (  $\diamond$  )  $CeVO_4$ , ( \* ) Support,

**Table 1.** XRD Study for different oxygen carriers

Oxygen Carrier	Surface area (m <sup>2</sup> /g)	Pore volume (cm <sup>3</sup> /g)	Pore size (nm)	average crystallite size (nm)	
				Support	$V_2O_5$
TiO <sub>2</sub>	11.3	0.07	26.6	-	-
SiO <sub>2</sub>	7.0	0.014	14.4	-	-
Al <sub>2</sub> O <sub>3</sub>	153.9	0.508	9.3	-	-
ZrO <sub>2</sub>	22.3	0.012	3.0	-	-
CeO <sub>2</sub>	61.6	0.099	5.5	-	-
$V_2O_5/TiO_2$	7.2	0.058	61.5	88	51
$V_2O_5/SiO_2$	1.6	0.025	46.0	-	87
$V_2O_5/Al_2O_3$	118.8	0.365	9.0	10	59
$V_2O_5/ZrO_2$	21	0.025	5.2	32	57
$V_2O_5/CeO_2$	23.0	0.062	7.6	12	51

(↓) SiC; "AR" indicates samples after reaction (in red).

### Temperature programmed reduction

TPR of bulk and supported  $V_2O_5$  show the presence of several peaks at different temperatures that suggest the stepwise reduction of the  $V_2O_5$  species which is present initially<sup>[18]</sup> but at a lower temperature with respect to bulk  $V_2O_5$ . Bond et al.<sup>[32]</sup> stated that at high loading of the vanadium on  $TiO_2$  generates paracrystalline  $V_2O_5$  species, which show reduction at a lower temperature.

On the other hand, A. Klisińska et al. explained<sup>[33]</sup> that multiple reduction peaks located at 461, 661, 698 and 860 °C could be attributed to successive steps of the reduction to  $V_2O_3$  via  $V_6O_{13}$  and  $V_2O_4$ , or/and to the heterogeneity of V–O which are reduced. The  $TiO_2$  based solid exhibits four different peaks at 478 °C, 588 °C, 654 °C, and 750 °C which can represent the successive steps of the reduction of the  $V^{5+}$  to  $V^{4+}$ . However, peaks at 480 °C can be due to the reduction of the  $V^{5+}$  or the slightly impure  $TiO_2$ , as suggested by Bond et al.<sup>[32]</sup>

Ceria based solid exhibits a peak at 573 °C, which can correspond to the reduction of polyvanadate or crystalline  $V_2O_5$  whereas peaks at high temperatures at 719 °C and 828 °C corresponds to the reduction of the ceria species as shown by X. Gu et al.<sup>[34]</sup> Lian et al.<sup>[35]</sup> also attributes the reduction at the high temperature to bulk ceria, whereas Yasyerli et al.<sup>[36]</sup> proposed that the broad peak obtained at high temperature corresponds to the removal of oxygen from  $CeVO_4$ , resulting in the reduction of  $V^{5+}$ .

Zirconia based solid shows a peak at 448 °C, illustrating the reduction of the  $V_2O_5$  species. However, the peak at high temperature represents the reduction at  $ZrO_2$ .<sup>[37]</sup>

For the alumina-based solid, in the TPR profile shows a peak present at the 570 °C attributed to the reduction of  $V^{5+}$  to  $V^{4+}$  ( $V_2O_4$ ). The reduction peak for  $Al_2O_3$  is absent in the spectrum. [38,39] Al-Ghamdi et al.<sup>[37,39]</sup> assigned the peak at 570 °C to the reduction of bulk  $V_2O_5$ -like surface species.

Finally, the TPR profile of  $SiO_2$  based solid shows the presence of only one broad peak centered at 651 °C.

The reduction temperature of vanadium species supported on all supports is lower than that of bulk  $V_2O_5$ , which indicates that even if high loadings are considered, the interaction between active phase and support are critical factors in the reducibility of vanadium species.

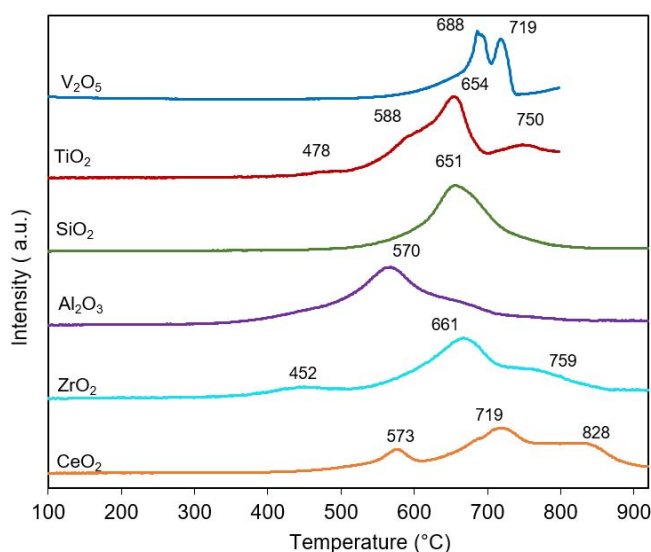


**Table 2.** H<sub>2</sub> Consumption for supported oxygen carriers

Oxygen Carrier (25 wt % V <sub>2</sub> O <sub>5</sub> )	H <sub>2</sub> consumption (mmol/g)
Support	
TiO <sub>2</sub>	1.26
SiO <sub>2</sub>	2.81
Al <sub>2</sub> O <sub>3</sub>	2.36
ZrO <sub>2</sub>	1.14
CeO <sub>2</sub>	3.50

**Figure 2.** TPR study for bulk of supported (25 wt% V<sub>2</sub>O<sub>5</sub>) oxygen carriers.

### XPS analysis

The V 2p<sub>3/2</sub> and the O 1s XPS spectra were analyzed to determine the oxidation state of the vanadium impregnated on different supports.

After deconvolution of the peaks for the different solids, it is evident that only V<sup>5+</sup> and V<sup>4+</sup> species are present in the systems. For example, in the case of SiO<sub>2</sub> based solid, two peaks are observed at a binding energy of 517.4 eV, which represents the V<sup>5+</sup> species, and at 516.0 eV, illustrating the presence of V<sup>4+</sup> species (Figure 3). TiO<sub>2</sub> based solid presents the highest amount of V<sup>4+</sup> compared to other solids, followed by SiO<sub>2</sub>, ZrO<sub>2</sub>, CeO<sub>2</sub>, and finally, Al<sub>2</sub>O<sub>3</sub>.

V/Support ratio for TiO<sub>2</sub>, SiO<sub>2</sub>, Al<sub>2</sub>O<sub>3</sub> are almost the same. It is slightly higher for ZrO<sub>2</sub>, but the maximum ratio is observed in the case of the ceria based solid (around 2.65) (Table 3), which

correlates well with the presence of the big particle size of the vanadium phase on the surface of this support.

Regarding oxygen, three species are observed. However, the explanation is not as simple as the total oxygen content is not straightforward. Generally, peak at 530.6 eV is attributed to O in vanadium oxide.<sup>[40]</sup> In the case of the SiO<sub>2</sub> supported carrier, different oxygen species are present. From the deconvolution of the spectra, two components representing different chemical states are recognized. The peak at 532.6 eV illustrates the presence of the oxygen connected to the Si in SiO<sub>2</sub>.<sup>[40,41]</sup> So, detected oxygen is mostly involved in the SiO<sub>2</sub> than V<sub>2</sub>O<sub>5</sub>. In the case of TiO<sub>2</sub> based carrier, peak at 529.9 eV is attributed to oxygen from TiO<sub>2</sub>.<sup>[42]</sup> The peak at 531.3 eV exhibits the presence of the O in TiO<sub>2</sub> or indicates the presence of Ti<sub>2</sub>O<sub>3</sub><sup>[43,44]</sup> while 533 eV is due to adsorbed molecular water.<sup>[5]</sup> In case of alumina-based catalyst, 531.4 eV peak is attributed to the oxygen from Al<sub>2</sub>O<sub>3</sub>.<sup>[41]</sup>

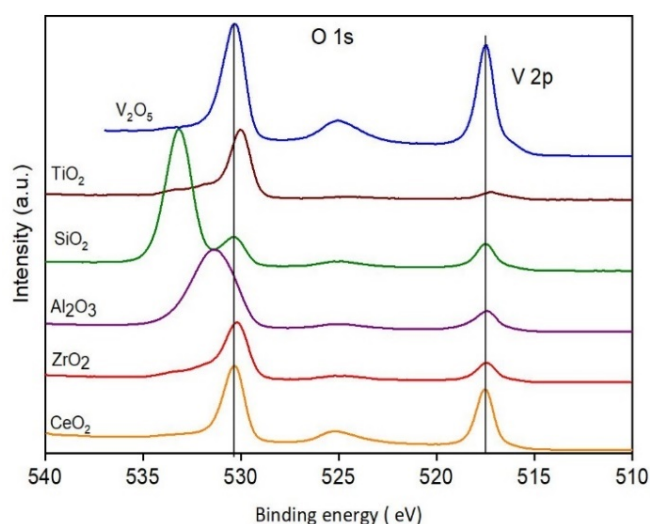


**Figure 3.** XPS study of the V 2p<sub>3/2</sub> and the O 1s of bulk of supported (25 wt% V<sub>2</sub>O<sub>5</sub>) oxygen carriers.

**Table 3.** XPS study of the V 2p<sub>3/2</sub> and the O 1s XPS on supported (25 wt% V<sub>2</sub>O<sub>5</sub>) carriers

Support	B.E. (eV)			V <sup>4+</sup> / (V <sup>4+</sup> + V <sup>5+</sup> )	V <sup>5+</sup> / (V <sup>4+</sup> + V <sup>5+</sup> )	V/support	V/O
	O 1s						
	O 1s	O 1s	O 1s				
TiO <sub>2</sub>	529.3	531.3	533	0.23	0.7	0.21	0.09
SiO <sub>2</sub>	530	-	533.1	0.10	0.9	0.18	0.44
Al <sub>2</sub> O <sub>3</sub>	-	531.4	-	*	1	0.19	0.1
ZrO <sub>2</sub>	530.1	531.3	533	0.07	0.9	0.35	0.18
CeO <sub>2</sub>	530.3	531.4	-	0.06	0.9	2.65	0.36

### Raman

The narrow peak at  $996\text{ cm}^{-1}$ , due to the symmetric stretching vibrations of V-O groups, is characteristic of crystalline  $\text{V}_2\text{O}_5$  (dashed lines, Figure 4). Additional bands observed near  $705\text{ cm}^{-1}$  arise from the stretching vibrations of V-O in the square octahedron of  $\text{V}_2\text{O}_5$ . The peaks at 284, 304, 483, 702, and  $997\text{ cm}^{-1}$  observed on all supports are thus attributable to different crystalline  $\text{V}_2\text{O}_5$  species.

For the  $\text{ZrO}_2$  solid, peak present at  $996\text{ cm}^{-1}$  can also coincide with the formation of the  $\text{ZrV}_2\text{O}_7$ .<sup>[37]</sup> Nevertheless, the presence of the surface  $\text{V}_2\text{O}_5$  can reasonably be supposed. The peak present at  $469\text{ cm}^{-1}$  on  $\text{CeO}_2$  supported carrier can be attributed to the presence of the  $\text{CeVO}_4$ , which is also confirmed by a low-intensity peak at  $866\text{ cm}^{-1}$ .<sup>[45,46]</sup>

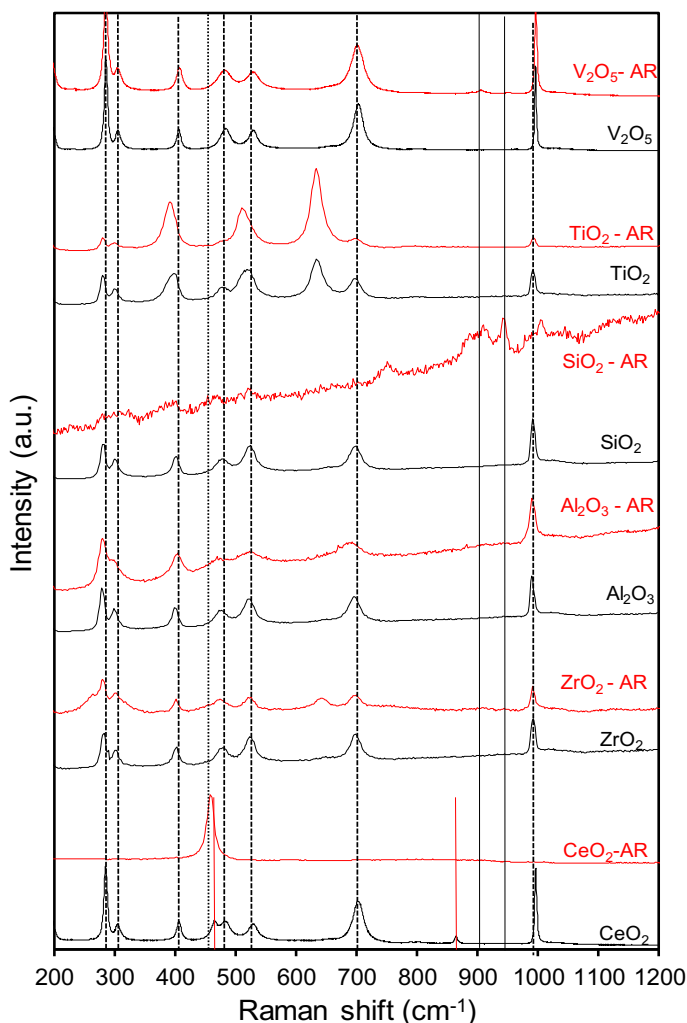


**Figure 4.** Raman study for bulk or supported (25 wt%  $\text{V}_2\text{O}_5$ ) oxygen carriers before and after the reaction, (...)  $\text{VO}_2$ , (—)  $\text{V}_4\text{O}_9$ , (---)  $\text{V}_2\text{O}_5$ , (—)  $\text{CeVO}_4$  "AR" indicates samples after reaction (in red).

For  $\text{TiO}_2$  based carrier, the bands at 195, 400, 530, and  $640\text{ cm}^{-1}$  are due to anatase. These coincide with the 133, 393, and  $530\text{ cm}^{-1}$  peaks of  $\text{V}_2\text{O}_5$  and make it difficult to distinguish between the prominent species present for anatase and crystalline  $\text{V}_2\text{O}_5$ .

Overall solid shows the presence of the formation of the dominant crystalline  $\text{V}_2\text{O}_5$  in all cases due to the presence of the high loading of the active phase over the surface of all the supports.

After the reaction, for  $\text{SiO}_2$  based carrier, new peaks appear at  $942\text{ cm}^{-1}$  attributed to the stretching of vanadyl bonds  $\text{V}(\text{b})=\text{O}(1\text{b})$ . The new peak at  $950\text{ cm}^{-1}$  is attributed to the stretching vibrations of  $\text{V}^{4+}=\text{O}$  bonds. After reaction  $\text{SiO}_2$  carrier shows the presence of the more  $\text{V}_4\text{O}_9$  species (solid lines, Figure 4) than before reaction. A higher oxygen deficiency is associated with an increase in the number of  $\text{V}^{4+}=\text{O}$  bonds as studied and explains by P. Shvets et al.<sup>[47]</sup> The asymmetric stretching of V-O-V bridges occur at  $753\text{ cm}^{-1}$ . A small intense peak present at  $464\text{ cm}^{-1}$  is assigned to V-O-V stretching modes from  $\text{VO}_2$  species. After reaction, alumina supported carrier exhibits bands attributed to  $\text{V}_2\text{O}_5$  species only. Reduced  $\text{VO}_x$  species ( $\text{V}_4\text{O}_9$  or  $\text{VO}_2$ ) are not observed contrary to the XRD. This would suggest that  $\text{V}_2\text{O}_5$  species are most abundant but in the amorphous form together with some crystallized reduced  $\text{VO}_x$ .

Zirconia-based carrier shows a similar peak before and after the reaction, with the exception of a peak at  $642\text{ cm}^{-1}$  attributed zirconia species.<sup>[48]</sup>

### Reactivity in chemical looping $\text{H}_2\text{S}$ selective oxidation

#### Reactivity of supports

Before studying the properties of supported carriers, experiments were performed on supports without the active phase. Results on the last stable cycle on  $\text{TiO}_2$ ,  $\text{SiO}_2$ , and  $\text{CeO}_2$ ,  $\text{Al}_2\text{O}_3$  and  $\text{ZrO}_2$  are summarized in Table 4 and Figure 5.

$\text{CeO}_2$  shows almost total conversion with very high selectivity towards  $\text{SO}_2$  in the reductant step. This demonstrates that ceria support itself plays the role of the oxygen carrier, although it is unselective.

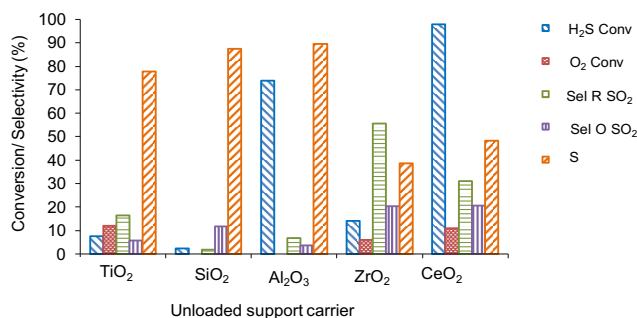


**Figure 5.** Overall reactivity (%ages) of unloaded supports at  $150\text{ }^\circ\text{C}$

**Table 4.** Reactivity of supports ( $150\text{ }^\circ\text{C}$ )

Unloaded support	$\text{H}_2\text{S}$ Conversion (%)	$\text{SO}_2$ Selectivity (%)
$\text{TiO}_2$	7 (28 cy)	22 (28 cy)
$\text{SiO}_2$	3 (9 cy)	13 (9 cy)
$\text{Al}_2\text{O}_3$	74 (10 cy)	10 (28 cy)
$\text{ZrO}_2$	14 (10 cy)	61 (10 cy)
$\text{CeO}_2$	98 (28 cy)	52 (28 cy)

Al<sub>2</sub>O<sub>3</sub> shows a high conversion of H<sub>2</sub>S with very low production of SO<sub>2</sub> in both steps. In this case, support plays a vital role in adsorbing the H<sub>2</sub>S due to its high surface area but shows low reactivity suggesting that sulfur species could accumulate on the support.

ZrO<sub>2</sub> shows the very low conversion of H<sub>2</sub>S with high selectivity towards SO<sub>2</sub>. This demonstrates that the ZrO<sub>2</sub> can also act directly as an unselective oxygen carrier but to a lower extent than CeO<sub>2</sub>.

Reactivity of the TiO<sub>2</sub> and SiO<sub>2</sub> supports are almost the same as illustrated in Figure 5. Low conversion of H<sub>2</sub>S and rather a low selectivity towards SO<sub>2</sub> are observed. However, in the case of TiO<sub>2</sub>, SO<sub>2</sub> is principally formed in the reductant step, which indicates that TiO<sub>2</sub> can act, to some extent, as an oxygen carrier. On the contrary, for SiO<sub>2</sub>, SO<sub>2</sub> is most formed in the oxidant step suggesting the oxidation by dioxygen of adsorbed sulfur containing species. In terms of selectivity to S, values should be taken with caution. Indeed, the formation of the elemental sulfur is not observed directly but calculated by a mass balance between consumed H<sub>2</sub>S and SO<sub>2</sub> produced (see Experimental Section). For instance, at such low conversion, adsorption and accumulation of S species on the support cannot be excluded, in particular for Al<sub>2</sub>O<sub>3</sub>. For SiO<sub>2</sub> support, the conversion of H<sub>2</sub>S is low (around 5%), whereas, for TiO<sub>2</sub> support, H<sub>2</sub>S conversion reaches 10% by the end of the cycling.

### Reactivity of supported V<sub>2</sub>O<sub>5</sub>

Figure 6 summarizes the conversions and selectivity at 150 °C (expressed in percentage) of the different solids, while Table 5 provides quantitative results expressed in net amounts of reactant converted or products for a single cycle. In both cases, values correspond to last cycle performed. The detailed evolution of the reactivity with respect to the number of cycles for different supported and bulk V<sub>2</sub>O<sub>5</sub> is shown in Figure 7.

Corresponding results obtained at 200 °C are presented in Figures 8 and 9 together with Table 6.

With the exception of temperature, all experiments have been done in similar conditions, i.e., with 2000 ppm of H<sub>2</sub>S, 10000 ppm of O<sub>2</sub> and 1-minute exposure to each reactant. Carriers were mixed to SiC to reach similar bed volume for all samples. SiC was checked to exhibit no reactivity.

### Reactivity at 150°C

H<sub>2</sub>S conversion is very high for all solids, as they all exhibit initial conversions above 90% except for the Al<sub>2</sub>O<sub>3</sub> supported carrier (80%). The conversion evolves with cycling differently according to the nature of the support. The activity of the Al<sub>2</sub>O<sub>3</sub> supported carrier is stable, that on CeO<sub>2</sub> support increases. In other cases, the activity decreases progressively. This is particularly the case for ZrO<sub>2</sub>, while TiO<sub>2</sub> and SiO<sub>2</sub> show very similar evolutions from 100% to approx. 92-93% H<sub>2</sub>S conversion.

The singular behavior of ceria, for which conversion of H<sub>2</sub>S increases with cycles, could be due to the presence of CeVO<sub>4</sub> species in the solid, which may participate in the reaction and contribute to the over-oxidation to SO<sub>2</sub> as seen in Figure 7(B). Indeed, this solid exhibit the worst (highest) selectivity to SO<sub>2</sub> formation during the reductant step (SO<sub>2</sub>R = 10%). At the same

time, this solid also shows the highest amount of SO<sub>2</sub> formed during the oxidant step as can be seen in Figure 7(C), and thus the worst overall selectivity to S formation (Figure 7(D)).

SO<sub>2</sub> production is observed in the reductant step for Al<sub>2</sub>O<sub>3</sub>, ZrO<sub>2</sub> and CeO<sub>2</sub> supported V<sub>2</sub>O<sub>5</sub> as well as for bulk V<sub>2</sub>O<sub>5</sub>. As mentioned, the amount is slightly higher for CeO<sub>2</sub> supported V<sub>2</sub>O<sub>5</sub>, which suggests a contribution of the support as active carrier coherently with the reactivity observed on the bare support.

Interestingly very low amounts of SO<sub>2</sub>R are formed using TiO<sub>2</sub> and SiO<sub>2</sub> supports. These solids show nearly full selectivity to elemental S if one considers only the reductant step.

The amount of lattice oxygen involved in TiO<sub>2</sub> supported V<sub>2</sub>O<sub>5</sub> is slightly higher than that of bulk V<sub>2</sub>O<sub>5</sub> but is coherent with the lower amount of active phase used (80 mg for bulk and 200mg containing 25 wt% for supported samples, i.e. 50 mg V<sub>2</sub>O<sub>5</sub>) and the higher activity of the supported sample. For other samples, this amount decreases logically with decreasing conversion and/or increasing amount of SO<sub>2</sub> formed during oxidant step.

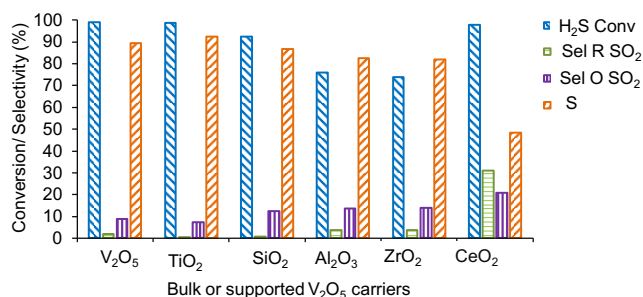
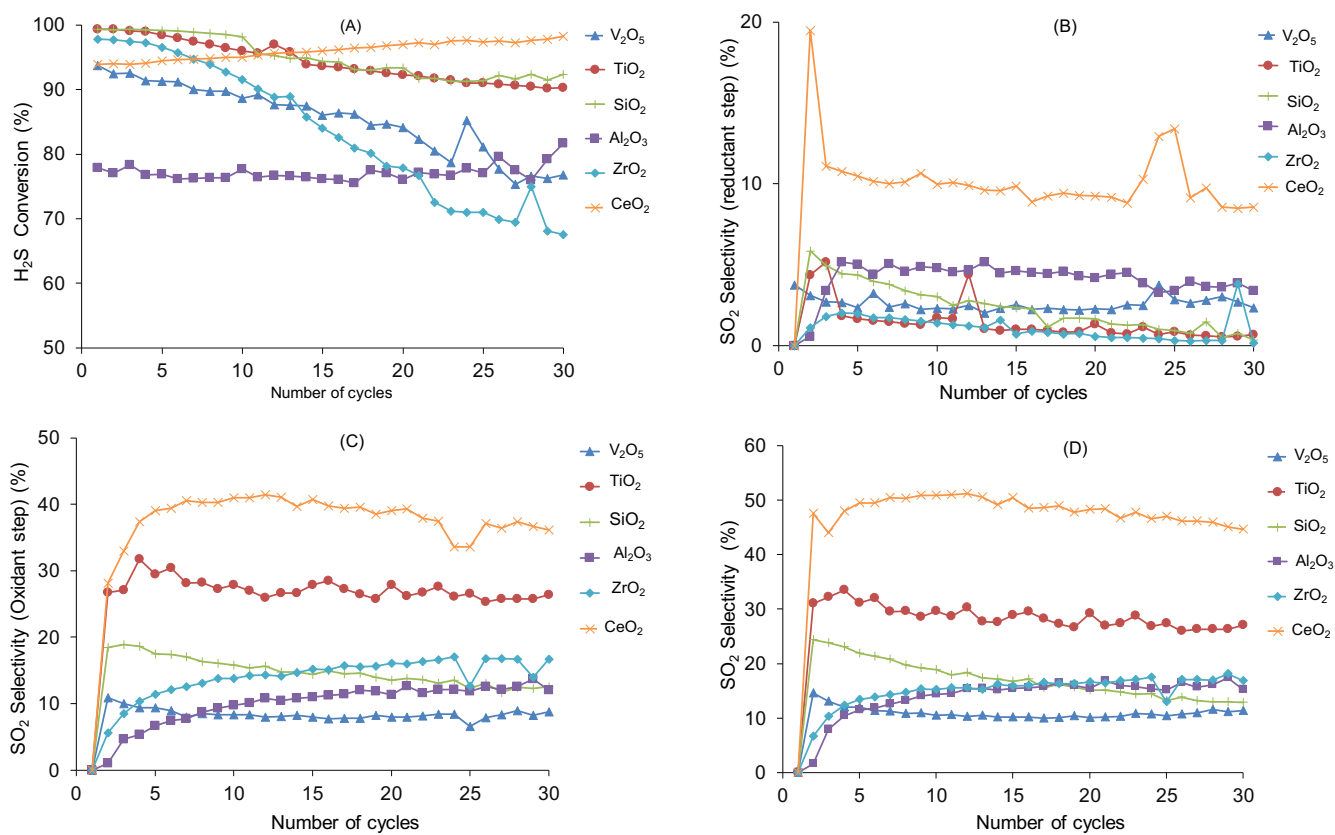


Figure 6. Overall reactivity (%ages) of bulk or supported V<sub>2</sub>O<sub>5</sub> at 150 °C.



**Figure 7.** Evolution of the reactivity of bulk or supported  $V_2O_5$  at  $150\text{ }^\circ\text{C}$ . A:  $H_2S$  conversion, B:  $SO_2$  selectivity in reductant step, C:  $SO_2$  selectivity in oxidant step, D: overall  $SO_2$  selectivity.

**Table 5.** Overall reactivity chemical looping (expressed in absolute amounts) at  $150\text{ }^\circ\text{C}$ .

Bulk or supported $V_2O_5$						
$150\text{ }^\circ\text{C}$	$V_2O_5$	$TiO_2$	$SiO_2$	$Al_2O_3$	$ZrO_2$	$CeO_2$
$H_2S$ feed ( $\mu\text{mol}$ )	8.6	8.6	8.6	8.6	8.6	8.6
% Conv $H_2S$	82	99	92	76	74	90
n converted ( $\mu\text{mol}$ )	7.05	8.74	7.94	6.94	6.36	7.92
S ( $\mu\text{mol}$ )	5.95	8.08	6.91	5.33	5.29	4.62
$SO_2R$ ( $\mu\text{mol}$ )	0.37	0.01	0.06	0.26	0.25	0.46
$SO_2O$ ( $\mu\text{mol}$ )	0.73	0.66	0.99	0.95	0.83	2.85
(S/S+ $SO_2R$ ) (%)	94	99	99	95	96	91
% $O_{latt}$ ( $V^{5+}$ to $V^{4+}$ )	1.60	2.8	2.45	2.14	2.11	2.06



## Reactivity at 200 °C

Figures 8 and 9 provide the reactivity results observed at 200 °C. Apart from Al<sub>2</sub>O<sub>3</sub> supported V<sub>2</sub>O<sub>5</sub>, H<sub>2</sub>S conversion increases for all carriers with respect to reaction performed at 150 °C. Generally, the selectivity to elemental S decreases significantly. SO<sub>2</sub> formed during reductant step increases for all samples, but particularly for TiO<sub>2</sub> and SiO<sub>2</sub> supported V<sub>2</sub>O<sub>5</sub>. At this temperature, bulk V<sub>2</sub>O<sub>5</sub> shows the best overall selectivity but suffers from significant deactivation contrary to supported samples.

As more lattice oxygen is required to form SO<sub>2</sub> than elemental S in the reductant step, the percentage of O<sub>latt</sub> logically increases in line with the lower selectivity (Table 6). This time, the amount of %O<sub>latt</sub> involved increases more for the supported sample than for bulk V<sub>2</sub>O<sub>5</sub>, even considering the lower amount of active phase used. The supports seem to induce higher oxygen mobility or reactivity compared to bulk V<sub>2</sub>O<sub>5</sub>.

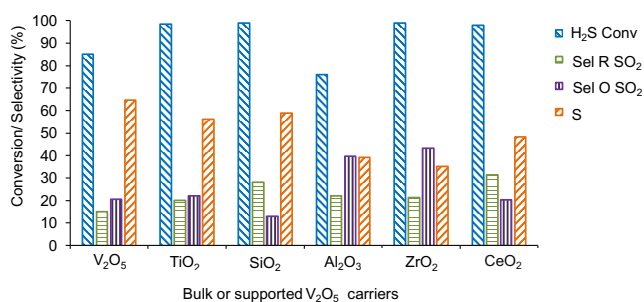


Figure 8. Overall reactivity (%ages) of bulk or supported V<sub>2</sub>O<sub>5</sub> at 200 °C.

## General discussion

Results show that the choice of support is crucial for the development of V<sub>2</sub>O<sub>5</sub> oxygen carriers for chemical looping selective oxidation of H<sub>2</sub>S. It will influence the reactivity of the active phase but can also play a role in the adsorption and activation of H<sub>2</sub>S. Indeed, H<sub>2</sub>S can form H-bond with surface OH groups of all the adsorbents. This adsorption phenomenon was studied and explained in detail by Travert et al. [49] for different supports like SiO<sub>2</sub>, Al<sub>2</sub>O<sub>3</sub>, TiO<sub>2</sub>, and ZrO<sub>2</sub>. This is the only way of adsorption of the H<sub>2</sub>S on SiO<sub>2</sub>, while other supports may lead to coordination as well as dissociative adsorption, which further leads to the formation of OH groups and molecular water. Specifically, on Titania, coordination to surface cations is predominant. These adsorbed H<sub>2</sub>S species can then either remain on the surface and be oxidized during the oxidant step of chemical looping, in this case producing SO<sub>2</sub> primarily or be oxidized by the support if it has some redox capacity. This is clearly seen in the case of TiO<sub>2</sub>, ZrO<sub>2</sub> and, mostly, CeO<sub>2</sub>.

Otherwise, the support mostly modifies the reactivity of V<sub>2</sub>O<sub>5</sub>. This is seen in TPR experiments for which, in case of all the supports, the reduction temperature is significantly lowered by the presence of support even if the crystallite size of V<sub>2</sub>O<sub>5</sub> is in the same range as that of bulk V<sub>2</sub>O<sub>5</sub>.

It was observed that the Al<sub>2</sub>O<sub>3</sub> supported V<sub>2</sub>O<sub>5</sub> shows the lowest initial reactivity (at 150 °C) and, with the exception of CeO<sub>2</sub> supported carrier, the highest selectivity towards SO<sub>2</sub> in reductant step compared to other supports (Figure 7b). This solid also exhibits the highest V<sup>5+</sup>/(V<sup>4+</sup> + V<sup>5+</sup>) initial ratio, as practically no V<sup>4+</sup> species were detected on the calcined solid by XPS. After the reaction, Al<sub>2</sub>O<sub>3</sub> supported carrier shows, by XRD, the disappearance of V<sub>2</sub>O<sub>5</sub> crystallites and the appearance of V<sub>4</sub>O<sub>9</sub> ones which indicates a strong reduction of the carrier during the chemical looping process. In contrast, Raman study on this support suggests that most vanadium species remain in V<sup>5+</sup> oxidation state. A possible explanation could be that most vanadium species are well dispersed at the surface of the support and in strong interaction with Al<sub>2</sub>O<sub>3</sub> thus remaining at high

oxidation state and exhibiting low reactivity. This is corroborated by the fact that the lowest amount of lattice oxygen (O<sub>latt</sub>) is actually involved on this sample, in particular at 200 °C (Table 6). Simultaneously, small crystallites presenting mostly reduced vanadium species are formed which could be responsible for the high reactivity but rather low selectivity towards partial oxidation of this carrier.

Interestingly, other supports show the presence of V<sup>4+</sup> species after calcination and high initial activity. In this respect, TiO<sub>2</sub> supported V<sub>2</sub>O<sub>5</sub> carrier has the highest proportion of V<sup>4+</sup> species and best initial activity. This carrier also exhibits among the best stability and selectivity in the reductant step. This suggests that the ability to maintain a good balance between V<sup>5+</sup> and V<sup>4+</sup> species between during the reaction is a crucial characteristic in order to achieve high performances in chemical looping. This is also observed in the case of SiO<sub>2</sub> supported V<sub>2</sub>O<sub>5</sub> although the decrease of V<sub>2</sub>O<sub>5</sub> phase and increase of V<sub>4</sub>O<sub>9</sub> phase are more intense which lowers the V<sup>5+</sup>/(V<sup>4+</sup> + V<sup>5+</sup>) ratio during reaction.

As mentioned, the CeO<sub>2</sub> supported V<sub>2</sub>O<sub>5</sub> behaves singularly compared to other supports. Contrary to others, the activity increases with time, but also selectivity worsens. This can evidently be attributed to the reactivity of CeO<sub>2</sub> but also CeVO<sub>4</sub> species.

These results are in line with those of Yasyerli et al. [50] and with M.Y Shin et al. [10] who showed that fully oxidized vanadium species lead to over oxidation to SO<sub>2</sub> whereas partially reduced V<sup>2+</sup> and V<sup>4+</sup> species lead to selective oxidation to elemental sulfur in classical (co-feed) catalytic reaction. Furthermore, Holgado et al. [30] have also proposed that V<sub>4</sub>O<sub>9</sub> phase characterized by V<sup>4+</sup>-O-V<sup>5+</sup> bonds is the most active, selective and stable for this reaction. Chemical looping reactivity agrees with these observations thus highlighting the importance of partially reduced vanadium species for this reaction.

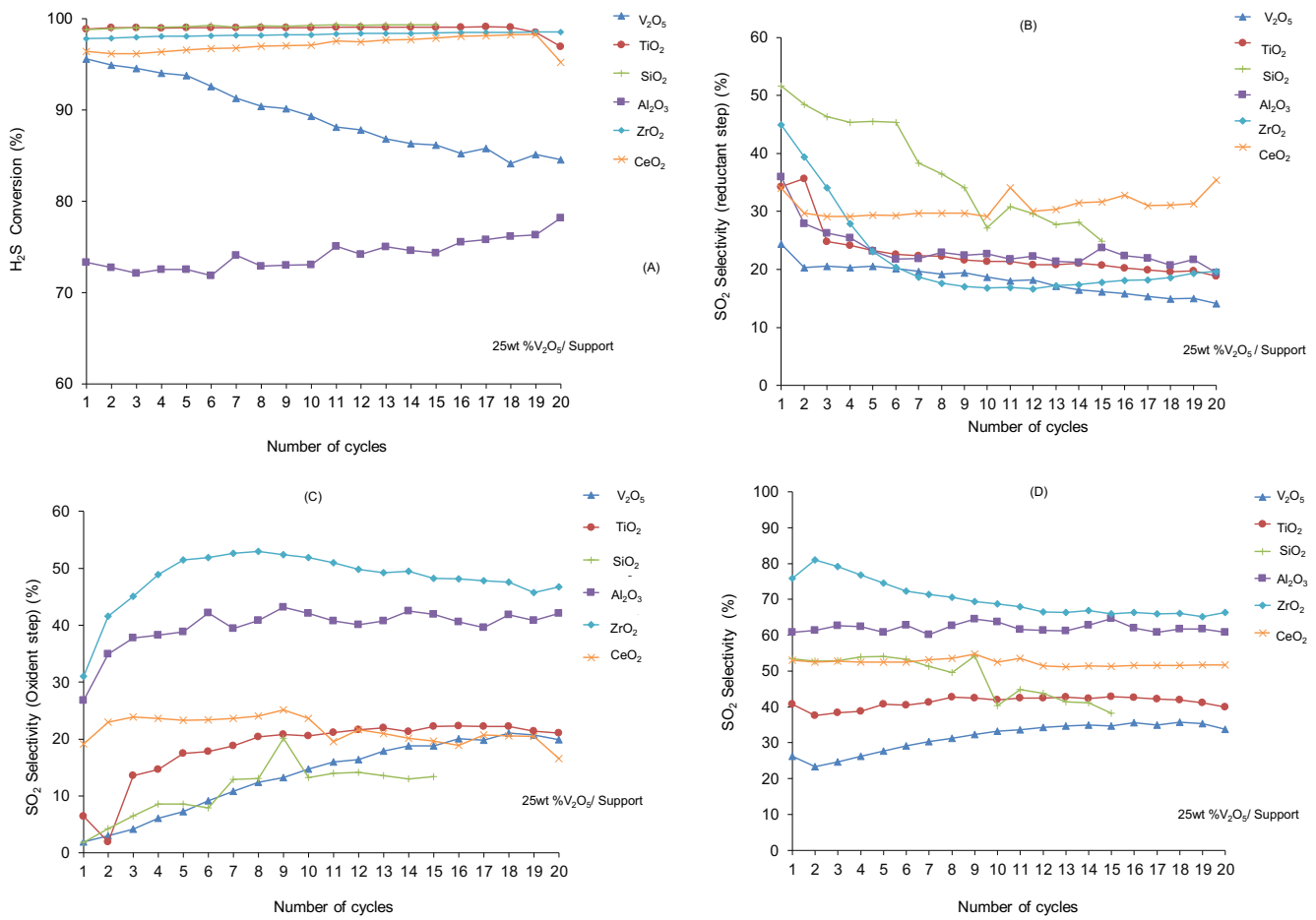


**Figure 9.** Evolution of the reactivity of bulk or supported  $V_2O_5$  at 200 °C. A:  $H_2S$  conversion, B:  $SO_2$  selectivity in reductant step, C:  $SO_2$  selectivity in oxidant step, D: overall  $SO_2$  selectivity.

**Table 6.** Overall reactivity chemical looping (expressed in absolute amounts) at 200 °C.

Bulk or supported $V_2O_5$						
200 °C	$V_2O_5$	$TiO_2$	$SiO_2$	$Al_2O_3$	$ZrO_2$	$CeO_2$
$H_2S$ feed ( $\mu\text{mol}$ )	8.6	8.6	8.6	8.6	8.6	8.6
% Conv $H_2S$	85	98.4	99	76	99	98
n converted ( $\mu\text{mol}$ )	7.31	8.71	8.51	6.54	8.51	8.62
S ( $\mu\text{mol}$ )	4.69	5.01	4.99	2.30	3.25	4.12
$SO_2R$ ( $\mu\text{mol}$ )	1.09	1.75	2.41	1.47	1.74	2.72
$SO_2O$ ( $\mu\text{mol}$ )	1.53	1.95	1.11	2.76	3.52	1.78
(S/S+ $SO_2R$ ) (%)	81	74	67	61	65	60
% $O_{\text{latt}}$ ( $V^{5+}$ to $V^{4+}$ )	1.81	3.60	4.23	2.36	2.99	4.23

## Conclusions

Selective oxidation of H<sub>2</sub>S in chemical looping mode offers interesting perspectives for improving the efficiency of existing H<sub>2</sub>S treatment processes. In previous work, V<sub>2</sub>O<sub>5</sub> had already been identified as a potential oxygen carrier for such a process. Here we have shown that supporting such an active phase can induce positive or detrimental effects according to the nature of the support and its interactions with the active phase. For instance, it appears clearly that TiO<sub>2</sub> and SiO<sub>2</sub> are the most interesting supports for V<sub>2</sub>O<sub>5</sub> for chemical looping selective oxidation of H<sub>2</sub>S. In both cases, the reactivity is increased as compared to bulk V<sub>2</sub>O<sub>5</sub>. In the case of TiO<sub>2</sub> support similar selectivity could also be reached while the amount of lattice O species involved increased meaning a better utilization of the oxygen capacity of the carrier. On other supports formation of some SO<sub>2</sub> during the reductant step could not be avoided.

A correlation between the presence of V<sup>4+</sup> and V<sup>5+</sup> species in the calcined samples and their reactivity in chemical looping H<sub>2</sub>S oxidation was found. Highly oxidized vanadium containing samples are less reactive and less selective to elemental sulfur while partially reduced species are more reactive but still maintain enough redox capacity to oxidize selectively H<sub>2</sub>S to elemental S. The best performances have been obtained on carriers in which both V<sub>2</sub>O<sub>5</sub> and V<sub>4</sub>O<sub>9</sub> coexist after reaction suggesting that selective oxidation occurs through the looping between V<sup>5+</sup> and V<sup>4+</sup> within these phases. The V<sub>2</sub>O<sub>5</sub>-support interactions appear to be determining to reach optimal balances between these phases as observed for TiO<sub>2</sub> and SiO<sub>2</sub> supports.

From these results, perspectives for the further development of selective vanadium-based oxygen carriers can be designed with an attention for TiO<sub>2</sub> and SiO<sub>2</sub> supported systems.

## Experimental Section

### Synthesis of the carriers

The active phase was impregnated on synthesized or commercial supports. Different supports were considered for the synthesis of catalysts like TiO<sub>2</sub>, CeO<sub>2</sub>, ZrO<sub>2</sub>, Al<sub>2</sub>O<sub>3</sub>, and SiO<sub>2</sub>.<sup>[7,17,38,51,52]</sup> Among these, TiO<sub>2</sub> and Al<sub>2</sub>O<sub>3</sub> are commercial supports from Sigma Aldrich. Other supports were synthesized in the laboratory with precipitation method using different hydrolysis additives.

Commercial support from Sigma-Aldrich shows traces of K which can have a strong effect on the Vanadium dispersion and its activity. Before using the support for the solid preparation, it was washed in water to remove this impurity. Support was mixed with water and stirred for 3 hours vigorously. The slurry was then centrifuged and dried at 100 °C overnight.

Ceria support was prepared in the laboratory by precipitation method using TEA (Tetraethyl ammonia). The ratio for Ce (NO<sub>3</sub>): TEA was 1:4 whereas that for methanol: TEA was maintained at 1:4. Solution (A) is Ceria nitrate and water whereas solution (B) is TEA with methanol. Initially, both solutions were stirred separately to form clear solutions. Solution A was then added to solution B dropwise with continuous stirring. The brown colored precipitate was observed in the beaker. This solution (slurry) was then stirred continuously for 24 hours. to form a uniform slurry. After 24 hours. Stirring, water was evaporated by continuous stirring at 80 °C. The sample was then dried at 80 °C overnight and then calcined at 500 °C for 5 hours in the presence of air.

Zirconia support was prepared by precipitation method using an ammonia solution (25%). The required amount of Zr (NO<sub>3</sub>) was dissolved in water and stirred for 15 mins to form a clear homogenous solution. 25% concentrated ammonia was then added slowly and dropwise into this clear solution. The dark brown precipitate was then observed. This solution

(slurry) was then stirred continuously for 24 hrs. to form a uniform slurry, which was then filtered and washed with water several times. The sample was then dried at 80 °C overnight and then calcined at 500 °C for 10 hours in the presence of air.

SiO<sub>2</sub> support was prepared in the laboratory by precipitation method using ammonia solution. The required amount of TEOS was dissolved in ethanol-water mixture and stirred for 30 mins to form a clear homogenous solution. 25% concentrated ammonia was then added slowly and dropwise into this clear solution. The White colored precipitate was then observed. This solution (slurry) was then stirred continuously for 2 hours to form a uniform slurry. The obtained slurry was then filtered and washed with water several times till to have a neutral pH of the filtrate. The final sample was then dried at 80 °C overnight and then calcined at 500 °C for 10 hours in presence of air.

An active phase was deposited by the impregnation method. Ammonium metavanadate was used as a precursor for the synthesis process. The desired amount of precursor was mixed in 20 mL of distilled H<sub>2</sub>O. Then 1g of support was mixed with water and stirred. The precursor solution was then added to the solution which was stirred for 2 hrs. Continuously for aging and to make a uniform slurry. Afterward, water was evaporated, and the remaining slurry dried at 80 °C. Finally, the sample was calcined for 10 hrs. in the air at 500 °C using a ramping rate of 2°C/ min. In all cases, 25 Wt. % of V<sub>2</sub>O<sub>5</sub> was used for different supports.

### Characterization techniques

Oxygen carriers were analyzed before and after a chemical looping reaction to evaluate the structural or chemical changes.

For this purpose, a set of samples were submitted to 20 cycles of chemical looping in the following conditions: 2000 ppm of H<sub>2</sub>S in reductant step, 10000 ppm of O<sub>2</sub> in oxidant step, T= 200 °C. After the 20<sup>th</sup> cycle, the reaction was stopped (after the O<sub>2</sub> step) and the reactor was closed and cooled to room temperature. Samples collected after reaction are marked "AR".

The XRD patterns of the different catalysts were obtained by using a D8 Advanced Bruker AXS diffractometer. The wavelength of CuKα1 X-ray radiation used was 1.5418 Å. The configuration for Bragg-Brentano diffractometer was theta-2 theta. The samples were immobilized over the ceramic glass (Macor) holders. The angle (2θ) of XRD was varied between 10 and 80° with a step size of 0.02° and an integration time of 3 s.

N<sub>2</sub> physisorption at 77 K data were collected on a multipoint and monoint equipment to obtain the surface area of the different catalysts before and after the test.

XPS analysis was performed using a Kratos Analytical AXIS UltraDLD spectrometer. A monochromatized aluminum source (AlKα=1486.6 eV) was used for excitation. The X-ray beam diameter is around 1 mm. The analyzer was operated in constant pass energy of 40 eV using an analysis area of approximately 700×300 μm. Charge compensation was applied to compensate for the charging effect occurring during the analysis. The C 1s (2848 eV) binding energy (BE) was used as an internal reference. The spectrometer BE scale was initially calibrated against the Ag 3d5/2 (368.2 eV) level. The pressure was in the 10<sup>-10</sup> Torr range during the experiments. Simulation of the experimental photopeak was carried out using Casa XPS software. Quantification considered a nonlinear Shirley background subtraction.

Raman spectra were recorded at room temperature with the 647.1 nm excitation line from a Spectra Physics krypton ion laser with 3 mW laser power at the sample. The beam was focused on the compounds using the macroscopic configuration. The scattered light was analyzed with an XY 800 Raman Dilor spectrometer equipped with an optical multichannel detector (liquid nitrogen-cooled charge coupled device). The spectral resolution was approximately 0.5 cm<sup>-1</sup> in the investigated 200-1000 cm<sup>-1</sup> range.

### Chemical looping reactivity experiments

Chemical looping reaction was performed by exposing the solid alternatively to diluted H<sub>2</sub>S (2000 ppm) and O<sub>2</sub> (10000 ppm) maintaining a H<sub>2</sub>S:O<sub>2</sub> ratio of 1:5. Helium gas is mixed in the reactant as a diluent, and its overall concentration varies according to the change in the concentration of the reactant. Reactivity tests were done at 150 and 250 °C using either 200 mg of the supported carrier or 80 mg of bulk V<sub>2</sub>O<sub>5</sub>, diluted in inert material like SiC (800 and 900 mg SiC for supported or bulk V<sub>2</sub>O<sub>5</sub>, respectively).

In practice, between experiments, temperature treatments of the solids were performed by exposing the solid to diluted O<sub>2</sub> (1%) and heating the sample to 400 °C to remove adsorbed sulfur species and fully re-oxidize the carrier. In reaction conditions, premixed gas cylinders containing 1 mol% H<sub>2</sub>S in He and 10 mol% O<sub>2</sub> in He were used as well as pure Ar. Helium gas serves as a diluent as well as a tracer for conversion calculations as its overall concentration varies according to the change in the concentration of the reactants during cycling operations. Thus, a significant gas stream of H<sub>2</sub>S/He (5 mL.min<sup>-1</sup>) was passed through the reactor together with 85 mL.min<sup>-1</sup> of Ar during the so-called "reductant step" and O<sub>2</sub>/He (10 mL.min<sup>-1</sup>) together with 85 mL.min<sup>-1</sup> of Ar during so-called "oxidant step". Between these steps, a total of 100 mL.min<sup>-1</sup> Ar was passed through the reactor in order to maintain the reactor under a constant flow (FT = 100 mL.min<sup>-1</sup>). All flow rates were set using mass flow controllers (5980 Brooks).

A glass tube maintained at room temperature was placed at the outlet of the reactor in order to condensate the elemental sulfur produced and to avoid plugging of the mass spectrometer inlet.

Every single cycle involves the exposure of the sample to reductant (H<sub>2</sub>S) and oxidant (O<sub>2</sub>) for 1 min each with an interval of 2 min in Ar. Cycles were repeated 20 or 30 times. The reactor was closed during first and the last cycle of the reaction to get the reference bypass value for background definition and sensitivity determination for Ar, He, H<sub>2</sub>S and O<sub>2</sub> of the online quadrupole mass analyzer (Omnistar 200, Pfeiffer Vacuum). SO<sub>2</sub> sensitivity was determined and checked regularly using a calibrated gas mixture.

In reductant step, H<sub>2</sub>S conversion X<sub>H<sub>2</sub>S</sub> (%) is obtained by integrating the outlet H<sub>2</sub>S flow and comparing this to the theoretical H<sub>2</sub>S inlet calculated from the He tracer.

$$X_{H_2S} = \frac{(H_2S \text{ (inlet } (\mu\text{mol})) - H_2S \text{ (outlet } (\mu\text{mol})))}{H_2S \text{ (inlet } (\mu\text{mol}))} \times 100$$

In oxidant step, O<sub>2</sub> conversion X<sub>O<sub>2</sub></sub> (%) is obtained by integrating the outlet O<sub>2</sub> flow and comparing this to the theoretical O<sub>2</sub> inlet calculated from the He tracer.

$$X_{O_2} = \frac{(O_2 \text{ (inlet } (\mu\text{mol})) - O_2 \text{ (outlet } (\mu\text{mol})))}{O_2 \text{ (inlet } (\mu\text{mol}))} \times 100$$

SO<sub>2</sub> can be produced in both reductant and oxidant steps. S<sub>SO<sub>2</sub>R</sub> (%) represents SO<sub>2</sub> selectivity in reductant step (amount of SO<sub>2</sub> formed in presence of H<sub>2</sub>S and following inert gas divided by amount of converted H<sub>2</sub>S) and is indicative of direct unselective oxidation of H<sub>2</sub>S by the oxygen carrier.

$$S_{SO_2R} (\%) = \frac{SO_{2(R)} (\mu\text{mol})}{(H_2S \text{ (inlet } (\mu\text{mol})) - H_2S \text{ (outlet } (\mu\text{mol})))} \times 100$$

S<sub>SO<sub>2</sub>O</sub> (%) represents SO<sub>2</sub> selectivity in the oxidant phase (amount of SO<sub>2</sub> formed in presence of O<sub>2</sub> and following inert gas divided by amount of

converted H<sub>2</sub>S and represents the oxidation of sulfur species which remain adsorbed at the surface of the carrier after the reductant step.

$$S_{SO_2O} (\%) = \frac{SO_{2(O)} (\mu\text{mol})}{(H_2S \text{ (inlet } (\mu\text{mol})) - H_2S \text{ (outlet } (\mu\text{mol})))} \times 100$$

As S formation cannot be monitored directly from the mass spectrometer, the selectivity towards S can only be calculated indirectly considering the total SO<sub>2</sub> formed on the overall cycle and considering that no S accumulates on the carrier along cycling. Thus, S<sub>SO<sub>2</sub>T</sub> (%) represents the total SO<sub>2</sub> selectivity:

$$S_{SO_2T} = S_{SO_2R} + S_{SO_2O}$$

And selectivity to S is obtained as follows:

$$S_S = 100 - S_{SO_2T}$$

The amount of lattice oxygen (O<sub>latt</sub>) involved in the reductant step can be calculated considering the amount of S and SO<sub>2</sub> produced during the reductant step and taking into account the theoretical amount of corresponding H<sub>2</sub>O which should be produced which is an actual oxygen involved during the reduction of V<sup>5+</sup> to V<sup>4+</sup>.

## Acknowledgements

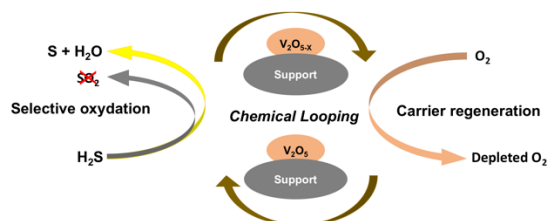
The Fonds Européen de Développement Régional (FEDER), CNRS, Région Hauts-de-France, Ministère de l'Education Nationale de l'Enseignement Supérieur et de la Recherche and Institut Chevreul are acknowledged for funding of XPS spectrometers and XRD instruments. TK and JGC are grateful to Univ. Lille and Région Hauts-de-France for providing financial support.

**Keywords:** H<sub>2</sub>S selective oxidation • V<sub>2</sub>O<sub>5</sub> • supported carriers • chemical looping • TiO<sub>2</sub>

- [1] X. Zhang, Y. Tang, S. Qu, J. Da, Z. Hao, *ACS Catal.* **2015**, *5*, 1053–1067.
- [2] K.T. Li, C.H. Huang, *Can. J. Chem. Eng.* **1999**, *77*, 1141–1145.
- [3] A. Corma, H. García, *Chem. Rev.* **2002**, *102*, 3837–3892.
- [4] A.A. Davydov, V.I. Marshneva, M.L. Shepotko, *App. Cat. A: Gen.* **2003**, *244*, 93–100.
- [5] B. Pongthawornsakun, S. Phatyenchuen, J. Panpranot, P. Praserttham, *J. Environ. Chem. Eng.* **2018**, *6*, 1414–1423.
- [6] M.D. Soriano, J.A. Cecilia, A. Natoli, J. Jiménez-Jiménez, J.M. López Nieto, E. Rodríguez-Castellón, *Catal. Today* **2015**, *254*, 36–42.
- [7] X. Zhanga, G. Doua, Z. Wang, L. Li, Y. Wang, H. Wang, Z. Hao, *Catal. Sci. Technol.* **2013**, *260*, 104–111.
- [8] K.-T. Li, T.-Y. Chien, *Catal. Lett.* **1999**, *57*, 77–80.
- [9] R.D. Solunke, G. Vesper, *Energy and Fuels* **2009**, *23*, 4787–4796.
- [10] M.Y. Shin, C.M. Nam, D.W. Park, J.S. Chung, *App. Catal. A: Gen.* **2001**, *211*, 213–225.
- [11] M.Y. Shin, D.W. Park, J.S. Chung, *Appl. Catal. B Environ.* **2001**, *30*, 409–419.
- [12] P. Kalinkin, O. Kovalenko, O. Lapina, D. Khabibulin, N. Kundo, *J. Mol. Catal. A Chem.* **2002**, *178*, 173–180.
- [13] M.W. Song, M. Kang, Kyung L K, *React. Kinet. Catal. Lett.* **2002**, *52*, 1–5.
- [14] J.D. Lee, N. Park, K.B. Han, S.O. Ryu, T.J. Lee, *Stud. Surf. Sci. Catal.* **2006**, *159*, 425–428.
- [15] K. V. Bineesh, D.R. Cho, S.Y. Kim, B.R. Jermy, D.W. Park, *Catal. Commun.* **2008**, *9*, 2040–2043.
- [16] J.S. Eow, *Environ. Prog.* **2002**, *21*, No.3, 143–162.
- [17] B.K. Vijayan, K.M. Il, L.G. Hwa, S. Manickam, P.D. Won, *Appl. Clay Sci.* **2013**, *74*, 127–134.
- [18] G.C. Bond, S.F. Tahir, *Appl. Catal.* **1991**, *71*, 1–31.
- [19] D.W. Park, B.K. Park, D.K. Park, H.C. Woo, *Appl. Catal. A, Gen.* **2002**, *223*, 215–224.
- [20] M. León, J. Jiménez-Jiménez, A. Jiménez-López, E. Rodríguez-Castellón, D. Soriano, J.M.L. Nieto, *Solid State Sci.* **2010**, *12*, 996–1001.
- [21] T. Mattisson, Martin Keller, C. Linderholm, P. Moldenhauer, M. Ryden, H. Leion, A. Lyngfelt, *Fuel Process. Technol.* **2018**, *172*, 1–12.
- [22] T. Kane, J. Guerrero-Caballero, A. Löfberg, *Appl. Catal. B: Environ.* **2020**, *265*, 118566.

- [23] Z. Guo, B. Liu, Q. Zhang, W. Deng, Y. Wang, Y. Yang, *Chem. Soc. Rev.* **2014**, *43*, 3480–3524.
- [24] A. Löfberg, J. Guerrero-Caballero, T. Kane, A. Rubbens, L. Jalowiecki-Duhamel, *Appl. Catal. B: Environ.* **2017**, *212*, 159–174.
- [25] S. Bhavsar, M. Najera, G. Veser, *Chem. Eng. Technol.* **2012**, *35*, No 7, 1281–1290.
- [26] J. Ma, C. Wang, H. Zhao, X. Tian, *Energy & Fuels* **2018**, *32*, 4493–4501.
- [27] R.F. Pachler, K. Mayer, S. Penthor, M. Kollerits, H. Hofbauer, *Int. J. Greenh. Gas Control.* **2018**, *71*, 86–94.
- [28] M.D. Soriano, A. Vidal-Moya, E. Rodríguez-Castellón, F. V. Melo, M.T. Blasco, J.M.L. Nieto, *Catal. Today* **2016**, *259*, 237–244.
- [29] J. Cecilia, M. Soriano, A. Natoli, E. Rodríguez-Castellón, J. López Nieto, *Materials* **2018**, *11*, 1562–1579.
- [30] J.P. Holgado, M.D. Soriano, J. Jiménez-Jiménez, P. Concepción, A. Jiménez-López, A. Caballero, E. Rodríguez-Castellón, J.M.L. Nieto, *Catal. Today* **2010**, *155*, 296–301.
- [31] R. Nilsson, T. Lindblad, A. Andersson, *Chem. Lett.* **1994**, *29*, 409–420.
- [32] G.C. Bond, J.P. Zurita, S. Flamerz, P.J. Gellings, H. Bosch, J.G. Van Ommen, B.J. Kip, *Appl. Catal.* **1986**, *22*, 361–378.
- [33] A. Klisińska, S. Loridant, B. Grzybowska, J. Stoch, I. Gressel, *App. Cat. A: Gen.* **2006**, *309*, 17–27.
- [34] X. Gu, J. Ge, H. Zhang, A. Auroux, J. Shen, *Thermochim. Acta* **2006**, *451*, 84–93.
- [35] Z. Lian, F. Liu, H. He, *Catal. Sci. Technol.* **2015**, *5*, 389–396.
- [36] S. Yasyerli, G. Dogu, T. Dogu, *Catal. Today* **2006**, *117*, 271–278.
- [37] F. Roozeboom, M.C. Mittelmeijer-Hazeleger, J.A. Moulijn, J. Medema, V.H.J. De Beer, P.J. Gellings, *J. Phys. Chem.* **1980**, *84*, 2783–2791.
- [38] E.P. Reddy, R.S. Varma, *J. Catal.* **2004**, *221*, 93–101.
- [39] S.A. Al-Ghamdi, H.I. De Lasa, *Fuel.* **2014**, *128*, 120–140.
- [40] L.G. Gerling, C. Voz, R. Alcubilla, J. Puigdollers, *J. Mater. Res.* **2017**, *32*, 260–268.
- [41] P.A. Zhdan, A.P. Shepelin, Z.G. Osipova, V.D. Sokolovskii, *J. Catal.* **1979**, *58*, 8–14.
- [42] R.P. Netterfield, P.J. Martin, C.G. Pacey, W.G. Sainty, D.R. McKenzie, G. Auchterlonie, *J. Appl. Phys.* **1989**, *66*, 1805–1809.
- [43] J. Mendiádua, R. Casanova, Y. Barbaux, *J. Electron Spectros. Relat. Phenomena* **1995**, *71*, 249–261.
- [44] B. Bharti, S. Kumar, H.N. Lee, R. Kumar, *Sci. Rep.* **2016**, *6*, 1–12.
- [45] M. V. Martínez-Huerta, J.M. Coronado, M. Fernández-García, A. Iglesias-Juez, D. G., J.L. Fierro, G. M.A. Bañares, *J. Catal.* **2004**, *225*, 240–248.
- [46] P. Intaphong, S. Jonjana, A. Phuruangrat, P. Pookmanee, S. Artkla, S. Thongtem, T. Thongtem, *Dig. J. Nanomater. Biostructures* **2015**, *10*, No 4, 1281–1287.
- [47] P. Shvets, O. Dikaya, K. Maksimova, A. Goikhman, *J. Raman Spectrosc.* **2019**, *50*, 1226–1244.
- [48] S. Benomar, A. Massó, B. Solsona, R. Issaadi, J.M. López Nieto, *Catalysts* **2018**, *8*, 126–144.
- [49] A. Travert, O. V. Manoilova, A.A. Tsyganenko, F. Maugé, J.C. Lavalley, *J. Phys. Chem. B.* **2002**, *106*, 1350–1362.
- [50] S. Yasyerli, G. Dogu, I. Ar, T. Dogu, *Chem. Eng. Sci.* **2004**, *59*, 4001–4009.
- [51] R.J.A.M. Terorde, P.J. Van Den Brink, L.M. Visser, A.J. Van Dillen, J.W. Geus, *Catal. Today* **1993**, *17*, 217–224.
- [52] S. Sadasivan, A.K. Dubey, Y. Li, D.H. Rasmussen, *J. Sol-Gel Sci. Technol.* **1998**, *12*, 5–14.

## Entry for the Table of Contents (Please choose one layout)



*Tanushree Kane, Jesús Guerrero, Axel Löffberg*

**Page No. – Page No.**

**Chemical looping selective oxidation of H<sub>2</sub>S using V<sub>2</sub>O<sub>5</sub> impregnated over different supports as oxygen carriers**

**Chemical looping is an innovative** approach that allows the selective oxidation of H<sub>2</sub>S to elemental sulfur without contact between O<sub>2</sub> containing stream and molecular oxygen opening the path for improved and safer processes. The utilization of supported oxygen carriers provides new opportunities for better selectivity towards sulfur.